Draft version July 29, 2017
Typeset using LaTeX **twocolumn** style in AASTeX61

GWEMOPT: OPTIMIZING SEARCHES FOR ELECTROMAGNETIC COUNTERPARTS OF GRAVITATIONAL WAVE TRIGGERS

Man Leong Chan,[1] Deep Chatterjee,[2] Michael Coughlin,[3] Shaon Ghosh,[2] Giuseppe Greco,[4] Yiming Hu,[5] Shasvath Kapadia,[2] Javed Rana,[6] Om Sharan Salafia,[7] and Duo Tao[8]

[1] *University of Glasgow, Glasgow G12 8QQ, United Kingdom*
[2] *University of Wisconsin-Milwaukee, Milwaukee, WI 53201, USA*
[3] *Department of Physics, Harvard University, Cambridge, MA 02138, USA*
[4] *INFN, Sezione di Firenze, I-50019 Sesto Fiorentino, Firenze, Italy*
[5] *TianQin Research Center for Gravitational Physics, Sun Yat-sen University, Tangjiawan, Zhuhai 519082, Guangdong, P. R. China*
[6] *Inter-University Centre for Astronomy and Astrophysics, Pune 411007, India*
[7] *INAF - Osservatorio Astronomico di Brera Merate, via E. Bianchi 46, I23807 Merate, Italy*
[8] *Carleton College, Northfield, MN 55057, USA*

ABSTRACT

Documentation for gwemopt

1. INTRODUCTION

There has been significant effort expended in the search for the electromagnetic counterpart of the gravitational waves found by compact binary black hole systems (Abbott et al. 2016; Abbott, B. P. et al. 2016; Abbott et al. 2017). In general, there is significant optimism for the potential counterparts for emission from binary neutron star and black hole - neutron star systems across timescales and wavelengths (Nakar 2007; Metzger and Berger 2012). The scientific output from a joint gravitational-wave and electromagnetic observation is expected to be significant. For example, detection of a kilonova coincident with a gravitational wave would allow for the exploration of r-process nucleosynthesis in the unbound ejecta from a merger involving a neutron star Metzger et al. (2015). In addition, a joint observation with a short gamma-ray burst would not only confirm that these phenomena are driven by compact binary mergers, but also allow for the study of their beaming, energetics, and galactic environment Metzger and Berger (2012).

To facilitate the detection of gravitational-wave counterparts, probability skymaps as a function of sky direction and distance are released for gravitational wave triggers produced by the detectors (Singer et al. 2014; Berry et al. 2015). Due to the significant sky coverage required to observe the gravitational-wave sky localization regions, usually spanning $\approx 100\,\mathrm{deg}^2$, techniques to optimize the followup efforts are of significant utility (Fairhurst 2009, 2011; Grover et al. 2014; Wen and Chen 2010; Sidery et al. 2014; Singer et al. 2014; Berry et al. 2015; Essick et al. 2015; Cornish and Littenberg 2015; Klimenko et al. 2016). Given the large sky localization regions involved, wide-field survey telescopes have the best opportunities to make a detection. The Panoramic Survey Telescope and Rapid Response System (Pan-STARRS) Morgan et al. (2012), Asteroid Terrestrial-impact Last Alert System (ATLAS) Tonry (2011), the intermediate Palomar Transient Factory (PTF) Rau et al. (2009) and (what will become) the Zwicky Transient Facility (ZTF), BlackGEM Bloemen et al. (2015) and the Large Synoptic Survey Telescope (LSST) Z. Ivezic et al (2014) are all examples of such systems. For example, Pan-STARRS has a 7° field of view (FOV), achieving a 5 σ limit of 21.5 (AB mag) in the i band in a 45 second exposure. ATLAS has a 29.2° field of view, achieving a 5 σ limit of 18.7 in the cyan band in a 30 second exposure. For comparison, LSST will have a $9.6\mathrm{deg}^2$ FOV and will require a 21 s r-band exposure length to reach 22 mag.

Due to the significant difference in telescope configurations, including FOV, filter, typical exposure times, and limiting magnitudes, in addition to placement on the earth and therefore different seeing and sky conditions, optimizing gravitational wave followups for generic telescopes is difficult. Therefore, in the following, we will take the telescopes mentioned above as examples.

For this reason, we have created a codebase named *gwemopt* that utilizes methods from a variety of recent papers geared towards optimizing efforts of followup. We employ methods to read gravitational-wave skymaps and the associated information made available from GraceDB [1], in addition to information about the telescopes to tile the sky, allocate available telescope time to the chosen fields, and schedule that time in a way that optimizes based on expected lightcurves. In section 2, we describe the algorithm. In section 3, we describe the performance of the algorithms. In section 4, we offer concluding remarks and suggest directions for future research.

2. ALGORITHM

Figure 1 shows the flowchart for the *gwemopt* pipeline, developed to optimize the efforts of electromagnetic followup of gravitational-wave events. *gwemopt* is developed in python, which has the benefit of interfaces to both LIGO's gravitational-wave candidate event database (GraceDB) and HEALPIX Górski et al. (2005), the format in which LIGO reports skymaps.

It uses events provided by gracedb in addition to information about the telescopes to creating tiles and optimize time allocations in the fields. It uses information about potential lightcurves from electromagnetic counterparts to schedule the available telescope time. In the following, we will describe the calculations that go into creating tiling, time allocations, and observing sequences from the skymaps. We will account for both diurnal and observational constraints and have the possibility of imaging over many nights.

2.1. *GraceDB*

```
python gwemopt_run --doEvent --do3D --event G268556
```

GraceDB is a service that provides information on candidate gravitational-wave events and the multi-messenger followups performed on them. An API is made available that allows for access to this information. *gwemopt* uses this API to access information pertinent for gravitational-wave followups. First of all, it downloads the gravitational-wave skymap for a given event; an example is shown in figure 2. In addition, in-

[1] https://gracedb.ligo.org

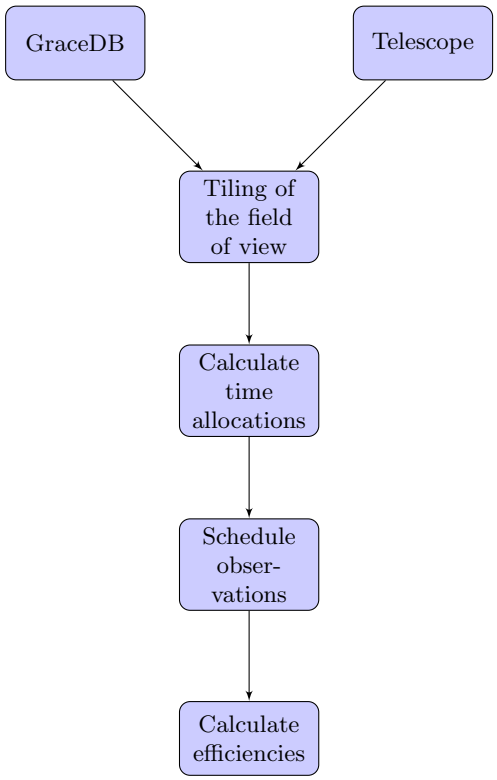

Figure 1. A flow chart of the *gwemopt* pipeline.

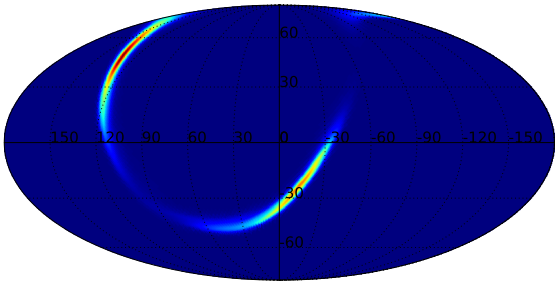

Figure 2. The gravitational-wave likelihood $L_{\rm GW}(\alpha, \delta, R)$ for GW170104.

formation such as the time of the event, the time delay between the time-of-arrival at the detectors, and (EM bright) information is noted.

2.2. *Telescope configuration*

```
python gwemopt_run --doEvent --do3D --telescope
    LSST
```

We require standardized configuration files for the telescopes to be analyzed. The information includes the filter being used, the limiting magnitude of the instrument and the exposure time required to achieve that magnitude, site location information, and information about the field of view shape and size. For the field of view, two options, square and circle are available, with the FOV being specified by the length of the square side and the radius of the circle. In addition, a tesselationFile is requested. This is especially useful for telescopes such as ZTF which use fixed telescope pointings which ensures the availability of reference images. In case a tesselation file is not available, one is automatically generated, described in the next section. Configuration files for ATLAS, BlackGEM, LSST, PS1, and ZTF are available. Table 1 provides the information assumed for these telescopes.

2.3. *Skymap tiling*

```
python gwemopt_run --doEvent --do3D --doTiles
    --doPlots --tilesType ranked
```

There are a variety of algorithms in the literature for sky-map tiling, and the ones implemented in *gwemopt* will be detailed below. The idea is to cover the sky with tiles the size of the telescope's field-of-view with minimal overlap. In some cases, these tiles are pre-determined by survey constraints in order to simplify difference imaging. In other cases, it is possible to optimize the tile locations based on the gravitational-wave skymaps, such that the tiles maximize the probability contained. In the following, we will check the difference between these tile locations to determine their effect. Due to the fields-of-view for these telescopes being in general much smaller than the probability region, the effect is expected to be relatively minimal.

Gravitational-wave skymaps in general contain metrics that report the spatial probability of a gravitational-wave source lying within a certain location. They are composed of HEALPIX arrays that encode either the 2D probability, in right ascension and declination, or 3D probability, which includes fits to the distance uncertainties. They are reported in particular number of pixels, usually $N_{\rm side} = 512$. This can introduce quantization errors, especially for small field-of-view telescopes. The –nside flag allows for the over- or under-sampling of the skymaps in the analysis. This can introduce quantization errors of (XXX) % for the field-of-view we consider here.

There are four options related to skymap tiling currently available, moc, ranked, hierarchical and greedy.

moc. Multi-order coverage of healpix maps hierarchically predefines cells in order to specify arbitrary sky regions Fernique et al. (2014).

Telescope	Latitude [deg]	Longitude [deg]	Elevation [m]	FOV [deg]	FOV shape	Filter	Exp. time [s]	Lim. Mag.
ATLAS	20.7204	-156.1552	3055.0	5.46	Square	c	30.0	18.7
Pan-STARRS	20.7204	-156.1552	3055.0	2.8	Circle	i	45.0	21.5
BlackGEM	-29.2612	-70.7313	2400.0	2.85	Square	g	300.0	23.0
LSST	-30.1716	-70.8009	2207.0	1.75	Circle	r	30.0	24.4
ZTF	33.3563	-116.8648	1742.0	6.86	Square	r	30.0	20.4

Table 1. Configuration of telescopes.

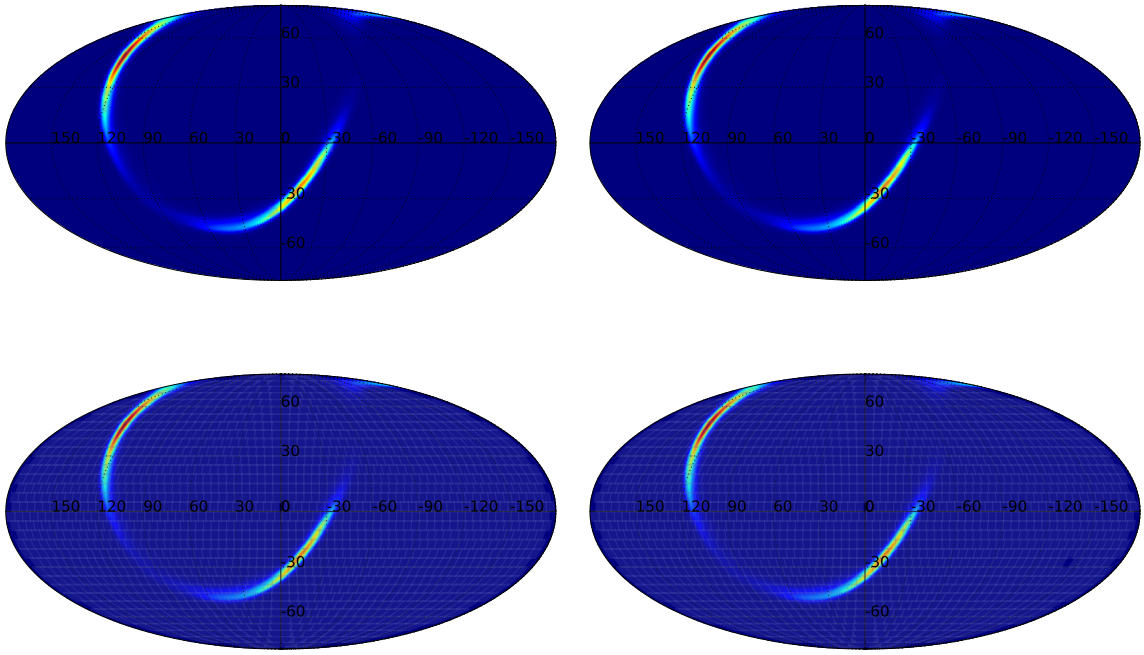

Figure 3. Example outputs of different tiling algorithms. On the top left is the greedy version with Ntiles = 10, on the top right is the hierarchical version with the same, on the bottom left is the MOC skymap, and on the bottom right is the ranked skymap tiling.

2.4. *Time allocations*

```
python gwemopt_run --doEvent --doPlots --doTiles
    --doSchedule -timeallocationType coverage
```

Once the tile locations have been assigned, whether dynamically or having been fixed previously, the next task is to assign time allocations to each tile, based on a variety of metrics. Because telescopes have fields of view that are in general significantly smaller than the probability region and typical exposure times for these telescopes are of order minutes (see Table 1), it is not possible to image the entire probability region to interesting limiting magnitudes in a reasonable amount of time. There are further constraints that arise from the diurnal cycle, observing time available for followup, limitations on the pointing a particular telescope is capable of, and the rise and set of tiles. The following algorithms use a variety of methods to optimize the probability of imaging a counterpart.

The amount of time allocated is defined by a few constraints. First of all, segments are generated based on the observing time allocated after the gravitational-wave event. In the analyses that follow, the default will be to assume the next 3 days are available. The segments are then intersected with night time at the site of the particular telescope. This defines the segments available for the analysis. The time available for the analysis is then determined from these segments. This assumes implicitly that the electromagnetic counterpart has not faded beyond detection limits in the time available. Some of the time allocation algorithms below will use models to determine when the counterpart is expected to be too faint to be detectable.

There are four options related to time allocations as a function of sky location available, powerlaw, WAW, PEM, and coverage.

Coverage. This is an option whereby coverage from existing surveys, including the right ascension and declination of the pointing and the limiting magnitude, are used.

Powerlaw. Many searches have used a variation on simply scaling the time allocation proportional to the probability skymaps, a technique employed in the Powerlaw method below. Coughlin and Stubbs Coughlin and Stubbs (2016) derived scaling relations for the time allocated to any given field, t_i, given the graviational-wave likelihood. We showed that under certain assumptions, $t_i \propto \left(\frac{L_{\rm GW}(\alpha_i,\delta_i)}{a(\alpha_i,\delta_i)}\right)^{2/3}$, where $L_{\rm GW}(\alpha_i,\delta_i)$ is the gravitational-wave likelihood and $a(\alpha_i,\delta_i)$ is Galactic extinction. While the powerlaw based analysis is straightforward, it does not account for the fact that the telescope must be sensitive enough to detect the counterpart. In this sense, this algorithm is the least model dependent. Although the detectability is model-dependent, both in the distances returned by the gravitational-wave detectors and the absolute magnitude of the sources, the following algorithms account for this in multiple ways.

WAW (Where and when). Salafia et al. Salafia et al. (2017) use counterpart lightcurve models in the optical, infrared and radio constructed from information from the gravitational-wave signals to create a time- and sky location dependent probability for detecting electromagnetic transients.

PEM (Probability of electomagnetic counterpart). Chan et al. Chan et al. (2017) optimize the number of fields to observe and their time allocations by adopting priors on the intrinsic luminosity of the sources and using knowledge of distance to the counterparts provided for compact binary coalescence.

2.5. *Scheduling*

```
python gwemopt_run --doEvent --doPlots --doTiles
    --doSchedule -scheduleType sear
```

Once the time allocated to each tile has been set, the next task is to schedule the observations that both best represent the time requested and optimize the times that are chosen in some way, for example, such that tiles are re-imaged at an approximately fixed cadence so as to measure possible lightcurve evolution or to go as deep as possible in one set. Other optimizations might employ ordering based on airmass, as sources imaged through higher airmass will have lower signal-to-noise ratios due to scattering.

The time that each tile is available for observation above the altitude limit is computed. Using the set of segments available to the telescope, these tile-specific segments are intersected with these segments to form a set of visibility segments for each tile. This has the benefit of avoiding issues related to simply tracking the rise and set times of each tile.

To account for lunar sky brightness, we use a model from Coughlin et al. Coughlin et al. (2016). Any tile whose sky brightness is increased by at least 1 mag is excluded.

There are three options related to scheduling observations, greedy, sear, and weighted.

Greedy. The simplest version of scheduling employs a schedule simply on the basis of probability contained. The idea is that higher ranked tiles are observed before lower ranked tiles based on this ranking scheme. Rana et al. Rana et al. (2017) implemented a greedy algorithm whereby the field with the highest probability region in a given time window is observed. As this analysis did not include the possibility of multiple exposures for each pointing, it is modified in the analysis to include multiple exposures. The algorithm is as follows:

1. Construct a list of the tiles and number of exposures for each tile based on the time allocation algorithm utilized.

2. For each window, find the sky tiles that are in the current window: $T_0 + (j-1)T_{exp}$ and $T_0 + jT_{exp}$

3. Allocate the window to the sky tile with the greatest probability, and increment the number of exposures for that tile down by 1.

sear (Setting Array). The greedy algorithm has the short-coming that it does not account for site visibility. This motivates re-ordering the sequence such that as many tiles can be imaged as possible. Rana et al. Rana et al. (2017) also implemented a version whereby the rising and setting of tiles were accounted for. It uses the idea that observes high probability tiles first, subject to the condition that each tile from the observing sequence must be observed before it sets.

weighted. Given the impossibility of necessarily observing all of the tiles as they rise and set given the requirement of using multiple exposures per tile, we are motivated to define a scheme whereby each tile is given a weight based on both gravitational-wave likelihood enclosed, the number of exposures required for that tile,

and the number of available slots for it to be image. Therefore we define the weights w_i as

$$w_i = L_{\rm GW}(\alpha_i, \delta_i) \times \frac{N_{\rm R}}{N_{\rm A}} \quad (1)$$

2.6. *Efficiency*

```
python gwemopt_run --doEvent --doPlots --doTiles
    --doSchedule --doEfficiency
```

We are able to test and compare the performance of these algorithms by performing simulated observations. We adopt observational constraints as follows. We use an observing limit of an altitude of 30°, corresponding to an airmass of 2.0. We assume observations are available to begin at twilight and dawn, corresponding to when the sun is 12° below the western and eastern horizons. We do not point away from the moon or account for sky brightness.

To estimate the efficiency for the "detection" of the electromagnetic counterparts to gravitational-wave transients, we perform simulated injections of supplied lightcurves. We provide example lightcurves for a variety of lightcurve models, including:

1. Tanaka et al. Tanaka et al. (2014): Simulations of binary systems showing ejecta morphology and resulting lightcurves. These simulations led to analytical models for black-hole neutron star systems from
2. Kawaguchi et al. Kawaguchi et al. (2016): Analytical models for black-hole neutron star systems based on Tanaka et al. Tanaka et al. (2014)
3. Dietrich and Ujevic Dietrich and Ujevic (2017): Analytical models for binary neutron star systems based on Tanaka et al. Tanaka et al. (2014)
4. Barnes et al. Barnes et al. (2016): Simulations of binary systems studying the emission profiles of radioactive decay products from the merger.
5. Metzger et al. Metzger et al. (2015): Blue "precursor" to the kilonovae driven by β-decay of the ejecta mass.

The requirements for "detection" of the electromagnetic counterparts to gravitational-wave transients are as follows. We require that the transient appear in (?) images over (?) nights. In each image, the transient must exceed the limiting magnitude in that image. The color of the transient is estimated from the filter given in the configuration file. We simulate the transients at a variety of location and distances consistent with the gravitational-wave probability skymap.

3. PERFORMANCE

4. CONCLUSION

5. ACKNOWLEDGMENTS

MC is supported by National Science Foundation Graduate Research Fellowship Program, under NSF grant number DGE 1144152.

REFERENCES

Benjamin P. Abbott et al. GW170104: Observation of a 50-Solar-Mass Binary Black Hole Coalescence at Redshift 0.2. *Phys. Rev. Lett.*, 118(22):221101, 2017. doi:10.1103/PhysRevLett.118.221101.

Abbott, B. P. et al. Gw151226: Observation of gravitational waves from a 22-solar-mass binary black hole coalescence. *Phys. Rev. Lett.*, 116:241103, Jun 2016. doi:10.1103/PhysRevLett.116.241103. URL http://link.aps.org/doi/10.1103/PhysRevLett.116.241103.

Abbott et al. Observation of gravitational waves from a binary black hole merger. *Phys. Rev. Lett.*, 116:061102, Feb 2016. doi:10.1103/PhysRevLett.116.061102. URL http://link.aps.org/doi/10.1103/PhysRevLett.116.061102.

Jennifer Barnes, Daniel Kasen, Meng-Ru Wu, and Gabriel Martnez-Pinedo. Radioactivity and thermalization in the ejecta of compact object mergers and their impact on kilonova light curves. *The Astrophysical Journal*, 829(2): 110, 2016. URL http://stacks.iop.org/0004-637X/829/i=2/a=110.

Berry et al. Parameter estimation for binary neutron-star coalescences with realistic noise during the advanced ligo era. *The Astrophysical Journal*, 804(2):114, 2015. URL http://stacks.iop.org/0004-637X/804/i=2/a=114.

S. Bloemen, P. Groot, G. Nelemans, and M. Klein-Wolt. The BlackGEM Array: Searching for Gravitational Wave Source Counterparts to Study Ultra-Compact Binaries. In S. M. Rucinski, G. Torres, and M. Zejda, editors, *Living Together: Planets, Host Stars and Binaries*, volume 496 of *Astronomical Society of the Pacific Conference Series*, page 254, July 2015.

Man Leong Chan, Yi-Ming Hu, Chris Messenger, Martin Hendry, and Ik Siong Heng. Maximizing the detection probability of kilonovae associated with gravitational wave observations. *The Astrophysical Journal*, 834(1):84, 2017. URL http://stacks.iop.org/0004-637X/834/i=1/a=84.

Neil J Cornish and Tyson B Littenberg. Bayeswave: Bayesian inference for gravitational wave bursts and instrument glitches. *Classical and Quantum Gravity*, 32 (13):135012, 2015. URL http://stacks.iop.org/0264-9381/32/i=13/a=135012.

Michael Coughlin and Christopher Stubbs. Maximizing the probability of detecting an electromagnetic counterpart of gravitational-wave events. *Experimental Astronomy*, pages 1–14, 2016. ISSN 1572-9508. doi:10.1007/s10686-016-9503-4. URL http://dx.doi.org/10.1007/s10686-016-9503-4.

Michael Coughlin, Christopher Stubbs, and Chuck Claver. A daytime measurement of the lunar contribution to the night sky brightness in lsst's ugrizy bands–initial results. *Experimental Astronomy*, 41(3):393–408, Jun 2016. ISSN 1572-9508. doi:10.1007/s10686-016-9494-1. URL https://doi.org/10.1007/s10686-016-9494-1.

Tim Dietrich and Maximiliano Ujevic. Modeling dynamical ejecta from binary neutron star mergers and implications for electromagnetic counterparts. *Classical and Quantum Gravity*, 34(10):105014, 2017. URL http://stacks.iop.org/0264-9381/34/i=10/a=105014.

Reed Essick, Salvatore Vitale, Erik Katsavounidis, Gabriele Vedovato, and Sergey Klimenko. Localization of short duration gravitational-wave transients with the early advanced ligo and virgo detectors. *The Astrophysical Journal*, 800(2):81, 2015. URL http://stacks.iop.org/0004-637X/800/i=2/a=81.

S. Fairhurst. Triangulation of gravitational wave sources with a network of detectors. *New Journal of Physics*, 11 (12):123006, December 2009. doi:10.1088/1367-2630/11/12/123006.

S. Fairhurst. Source localization with an advanced gravitational wave detector network. *Class. Quantum Grav.*, 28(10):105021, May 2011. doi:10.1088/0264-9381/28/10/105021.

P. Fernique, T. Boch, T. Donaldson, D. Durand, W. O'Mullane, M. Reinecke, and M. Taylor. MOC - HEALPix Multi-Order Coverage map Version 1.0. IVOA Recommendation 02 June 2014, June 2014.

K. M. Górski, E. Hivon, A. J. Banday, B. D. Wandelt, F. K. Hansen, M. Reinecke, and M. Bartelmann. HEALPix: A Framework for High-Resolution Discretization and Fast Analysis of Data Distributed on the Sphere. *ApJ*, 622: 759–771, April 2005. doi:10.1086/427976.

K. Grover, S. Fairhurst, B. F. Farr, I. Mandel, C. Rodriguez, T. Sidery, and A. Vecchio. Comparison of gravitational wave detector network sky localization approximations. *PhRvD*, 89(4):042004, February 2014. doi:10.1103/PhysRevD.89.042004.

Kyohei Kawaguchi, Koutarou Kyutoku, Masaru Shibata, and Masaomi Tanaka. Models of kilonova/macronova emission from black holeneutron star mergers. *The Astrophysical Journal*, 825(1):52, 2016. URL http://stacks.iop.org/0004-637X/825/i=1/a=52.

S. Klimenko, G. Vedovato, M. Drago, F. Salemi, V. Tiwari, G. A. Prodi, C. Lazzaro, K. Ackley, S. Tiwari, C. F. Da Silva, and G. Mitselmakher. Method for detection and reconstruction of gravitational wave transients with networks of advanced detectors. *Phys. Rev. D*, 93: 042004, Feb 2016. doi:10.1103/PhysRevD.93.042004. URL http://link.aps.org/doi/10.1103/PhysRevD.93.042004.

B. D. Metzger and E. Berger. What is the most promising electromagnetic counterpart of a neutron star binary merger? *The Astrophysical Journal*, 746(1):48, 2012. URL http://stacks.iop.org/0004-637X/746/i=1/a=48.

Brian D. Metzger, Andreas Bauswein, Stephane Goriely, and Daniel Kasen. Neutron-powered precursors of kilonovae. *Monthly Notices of the Royal Astronomical Society*, 446(1):1115, 2015. doi:10.1093/mnras/stu2225.

Jeffrey S. Morgan, Nicholas Kaiser, Vincent Moreau, David Anderson, and William Burgett. Design differences between the pan-starrs ps1 and ps2 telescopes. *Proc. SPIE*, 8444:84440H–84440H–15, 2012. doi:10.1117/12.926646. URL http://dx.doi.org/10.1117/12.926646.

Ehud Nakar. Short-hard gamma-ray bursts. *Physics Reports*, 442(16):166 – 236, 2007. ISSN 0370-1573. doi:http://dx.doi.org/10.1016/j.physrep.2007.02.005. URL http://www.sciencedirect.com/science/article/pii/S0370157307000476. The Hans Bethe Centennial Volume 1906-2006.

Javed Rana, Akshat Singhal, Bhooshan Gadre, Varun Bhalerao, and Sukanta Bose. An enhanced method for scheduling observations of large sky error regions for finding optical counterparts to transients. *The Astrophysical Journal*, 838(2):108, 2017. URL http://stacks.iop.org/0004-637X/838/i=2/a=108.

Arne Rau, Shrinivas R. Kulkarni, Nicholas M. Law, Joshua S. Bloom, David Ciardi, George S. Djorgovski, Derek B. Fox, Avishay Gal-Yam, Carl C. Grillmair, Mansi M. Kasliwal, Peter E. Nugent, Eran O. Ofek, Robert M. Quimby, William T. Reach, Michael Shara, Lars Bildsten, S. Bradley Cenko, Andrew J. Drake, Alexei V. Filippenko, David J. Helfand, George Helou, D. Andrew Howell, Dovi Poznanski, and Mark Sullivan. Exploring the optical transient sky with the palomar transient factory. *Publications of the Astronomical Society of the Pacific*, 121(886):1334, 2009. URL http://stacks.iop.org/1538-3873/121/i=886/a=1334.

O. S. Salafia, M. Colpi, M. Branchesi, E. Chassande-Mottin, G. Ghirlanda, G. Ghisellini, and S. Vergani. Where and when: optimal scheduling of the electromagnetic follow-up of gravitational-wave events based on counterpart lightcurve models. *ArXiv e-prints*, April 2017.

T. Sidery, B. Aylott, N. Christensen, B. Farr, W. Farr, F. Feroz, J. Gair, K. Grover, P. Graff, C. Hanna, V. Kalogera, I. Mandel, R. O'Shaughnessy, M. Pitkin, L. Price, V. Raymond, C. Röver, L. Singer, M. van der Sluys, R. J. E. Smith, A. Vecchio, J. Veitch, and S. Vitale. Reconstructing the sky location of gravitational-wave detected compact binary systems: Methodology for testing and comparison. *PhRvD*, 89(8): 084060, April 2014. doi:10.1103/PhysRevD.89.084060.

Leo P. Singer, Larry R. Price, Ben Farr, Alex L. Urban, Chris Pankow, Salvatore Vitale, John Veitch, Will M. Farr, Chad Hanna, Kipp Cannon, Tom Downes, Philip Graff, Carl-Johan Haster, Ilya Mandel, Trevor Sidery, and Alberto Vecchio. The first two years of electromagnetic follow-up with advanced ligo and virgo. *The Astrophysical Journal*, 795(2):105, 2014. URL http://stacks.iop.org/0004-637X/795/i=2/a=105.

Masaomi Tanaka, Kenta Hotokezaka, Koutarou Kyutoku, Shinya Wanajo, Kenta Kiuchi, Yuichiro Sekiguchi, and Masaru Shibata. Radioactively powered emission from black hole-neutron star mergers. *The Astrophysical Journal*, 780(1):31, 2014. URL http://stacks.iop.org/0004-637X/780/i=1/a=31.

J. L. Tonry. An Early Warning System for Asteroid Impact. *PASP*, 123:58, January 2011. doi:10.1086/657997.

L. Wen and Y. Chen. Geometrical expression for the angular resolution of a network of gravitational-wave detectors. *PhRvD*, 81(8):082001, April 2010. doi:10.1103/PhysRevD.81.082001.

Z. Ivezic et al. LSST: from science drivers to reference design and anticipated data products. *http://arxiv.org/abs/0805.2366*, 2014.